*Journal of Mechanical Engineering Research and Developments*
*ISSN: 1024-1752*
*CODEN: JERDFO*
*Vol. 44-, No. 5, pp. 207-218*
*Published Year 2021*

# Investigation of Aerodynamic Forces on Tracked Vehicles Affected by disturbing Winds

Marwa Y. Jleel and Haider J. Abid

Mechanical Engineering Department, University of Thi-Qar, Iraq.

*Corresponding Author Email: haider-jabaur-abid@utq.edu.iq

ABSTRACT

The self-driving car industry has taken great care to enhance road safety and driving experience by monitoring small distances between vehicles, among the factors that affect it is the distribution of winds . This paper will be studying the pressure and velocity distributions on the surface of the body of a passenger car (Chrysler300s) under the effect of wind at various angles (0o,35º, 90º, and 125º) when tracking another passenger car, as well as when tracking an SUV (Mercedes G-Class) car with three distances (5m,10m, and 15m) when the vehicle speed was 120 km / h and the air speed 80 km / h. Using CFX Ansys R (19.0) simulation program. The results showed that the largest value of the reaction force of the front tires is on the front right tire (Tire FR) of the passenger car at an angle of 35 o and a distance of 15 meters between the two tandem cars. The drag force of the two tandem cars decreases as the distance between them decreases and the drag force on the rear car is less than the front car because this may refer to that design of the Chrysler class does not generate significant wakes.

KEYWORDS

Drag Force, SUV, Aerodynamic, Chrysler300s.

## INTRODUCTION

The growing use of the Intelligent Transport System (ITS) will allow very close spacing of vehicles, which generally contributes to a reduction in net drag for the resulting convoys [1]. The force opposite to the direction of motion that affects a body moving through the air is aerodynamic drag. Drag force influences the speed and fuel efficiency of aircraft, road vehicles, or race cars as it acts in the opposite direction of motion [2]. Kazeroon et al (2014)[3] Over two close-following (tandem) cars at different speeds and different distances, three-dimensional flow computations have been studied. The drag force was discovered to be lower than the front one on the rear car. J Liu et al (2019)[4] 3D numeric simulation have been studied based on heavy lorries including cab, chassis and tyres. The findings suggest that there is an upwind pressure gradient in aerodynamic noise supplies. HE Xiaona et al (2019)[5] A CFD approach has been investigated for the establishment of a systematic external flow of passenger vehicles. The CD and Cl pattern for five models with varying underbody flattening levels demonstrates how important aerodynamic efficiency is to underbody flattening. Hammad et al (2019)[6] Aerodynamics have been studied in the presence and absence of a 30-degree crosswind on the stability of buses during the crossing of passenger cars.

In a crossing, the powers and moments of a passenger car change by up to 43%. L Prabhu et al (2020)[7] also researched reducing the drag force that helps to increase the use of fuel that contributes to environmental safety. To minimize the aerodynamic drag force, they used a Sedan vehicle with different kinds of spoilers. The vehicle architecture was conducted on SOLIDWORKS and was also used in SOLIDWORKS FLOW SIMULATION for the study. A A Markina et al (2020)[8] When using a series of cab carriages of various shapes, the aerodynamic drag coefficient for KAMAZ heavy trucks has been investigated. As a result, the fuel economy is determined from the aerodynamic drag coefficient, taking into account the preferred optimum cab fairing and cab-side extenders. P Kesuma et al (2020)[9] Analyses of Mobil Irit Tarumanagara's aerodynamic performance using CFD simulation have been tested and will be carried out in 3D on 3 different body models and 5-speed variants. Two flow parameters provided the results of the simulation; velocity and pressure indicating the best model for the body is body 3.

Abdul Basit et al (2020)[10] have researched aerodynamic and streamlining, drag strength, and lower lifting

force to minimise large motor work. The average drag coefficient is about 0.0950. O Arteaga et al (2020)[11] Aerodynamic analysis carried out on the bus bodywork by the program CFD, which culminated in a spoiler body, one with a front deflector and one with an original body; the second choice offered a higher lifting coefficient, decreased turbulence areas and an optimal drag coefficient aerodynamics. Abid and Hussein (2020) [12] The velocity and pressure distributions on the vehicle's body surface have studied at various angles under the influence of wind (35o, 90o, and 125o). As the wind was approaching the vehicle at an angle of 125 degrees, the measurements revealed the maximum torque and effort values.

OBJECTIVE

The objective of this work is to study the drag force exerted over the passenger car follow another passenger car and when fellow for an SUV with three distances of 5m,10m, and 15m between them, all states at differing angles (0º,35º, 90º, and 125º) under the impact of wind. For this analysis, CFD technology was used and ANSYS CFX R 19.0 was used as a tool.

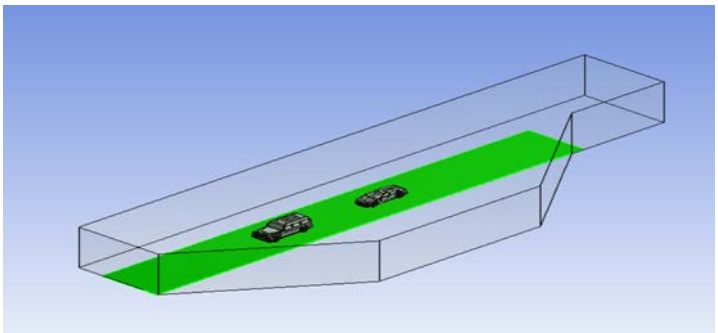

**Figure 1.** An illustration of angles of entry of wind

Mathematical Model

Conservation of mass (equation 1) and momentum (equation 2) are the primary governing equations. The above for the motion of the fluid is also known for the Navier-Stokes equation[12].

$$\frac{\partial \rho}{\partial t} + \frac{\partial (\rho u_i)}{\partial x_i} = 0 \tag{1}$$

$$\frac{\partial \rho u_i}{\partial t} + \frac{\partial (\rho u_i u_j)}{\partial x_j} = \frac{\partial \rho}{\partial x_i} + \frac{\partial}{\partial x_j}\left[\mu\left(\frac{\partial u_i}{\partial x_j} + \frac{\partial u_j}{\partial x_i}\right)\right] \tag{2}$$

Where

ui, uj are velocity components.
ρ is air density.
P is air pressure.
μ is dynamic viscosity.
and t is time.

The Stander K-e turbulence model was used. For the basic k-ε model, the transport conditions are:

$$\rho u_j \frac{\partial k}{\partial x_i} = \frac{\partial \varepsilon}{\partial x_j}\left((\mu + \frac{\mu_t}{\sigma\varepsilon})\frac{\partial \varepsilon}{\partial x_j}\right) + 2\mu_t S_{ij} . S_{ij} - \rho\varepsilon \tag{3}$$

$$\rho u_j \frac{\partial \varepsilon}{\partial x_j} = \frac{\partial \varepsilon}{\partial x_j}\left((\mu + \frac{\mu_t}{\sigma\varepsilon})\frac{\partial \varepsilon}{\partial x_j}\right) + C_{1\varepsilon}\frac{\varepsilon}{K}\mu_t S_{ij} . S_{ij} - C_{2\varepsilon}\rho\frac{\varepsilon^2}{K} \tag{4}$$

Where σk and σε are Prandtl numbers relating k and ε diffusivities of μt eddy viscosity, these values are σk=1.00 σε=1.30, Cμ=0.09, C1ε=1.44 and C2ε=1.92[13].

METHODOLOGY

CFD Analysis

The Analysis is carried out at a speed car is 120 km/h, and air velocity is 80 km/h in ANSYS-CFX R19.0. The analysis includes a process of steps:

Computational Domain:

It was positioned in the conceptual domain seen in figure 2 after the construction of the cars using a Solidwork program. These reflect the shapes and sizes of the computer studies areas for Chrysler car monitored together by Mercedes G-class car and two Chrysler vehicles, this is for domain applications for three spaces (5m,10m, and 15m) for both cases, and these shapes are modeled by ANSYS CFX 19.0.0 CFD software.

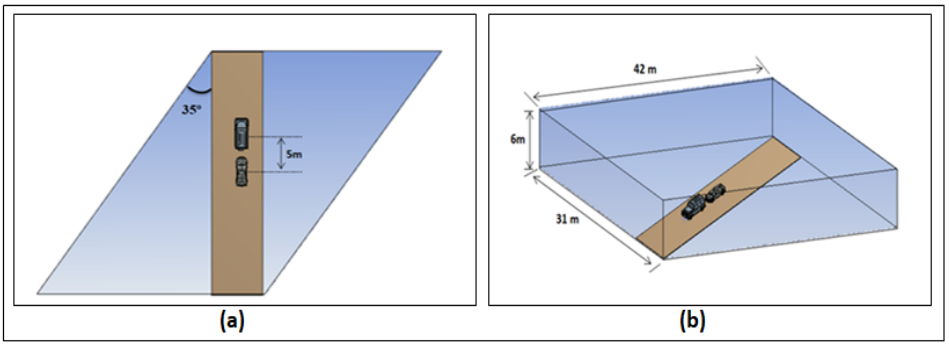


**Figure 2.** Computational range, (a) top view; (b) side view.

Meshing:

After drawing the studied model, the second appropriate step for finalizing the CFD simulation is to create the correct mesh. For this reason, ANSYS workbench (19.0) is used, because of the complexities of the structure of the car, only triangular meshing is used in ANSYS. Mesh is generated by the control limits shown in the figure3 on the vehicle body.

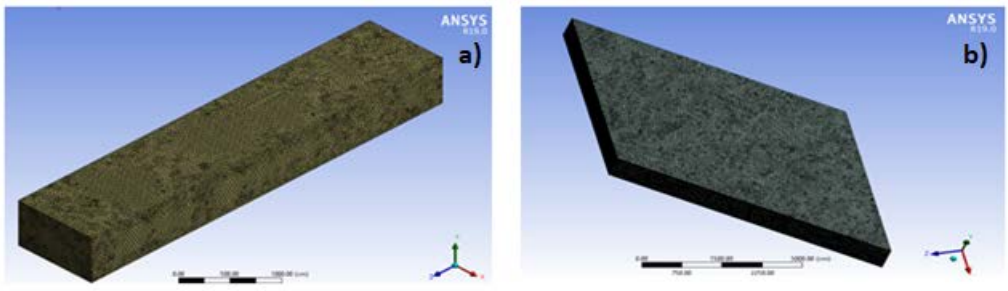


**Figure 3.** Mesh is generated on the car body by giving control limits, a) the influence of wind at 0o slip angle; b) the influence of wind at 35o slip angle.

Applying boundary conditions on the model of the vehicle:

As seen in figure 4, four states have been addressed in ANSYS CFX to decide for all states:

- State 1: One entry and one air raid on the cars.
- State 2: Two inlets here (front and wall with 35o slip angle).
- State 3: Two inlets here (front and wall with 90o slip angle).
- State 4: Two inlets here (front and wall with 125o slip angle).

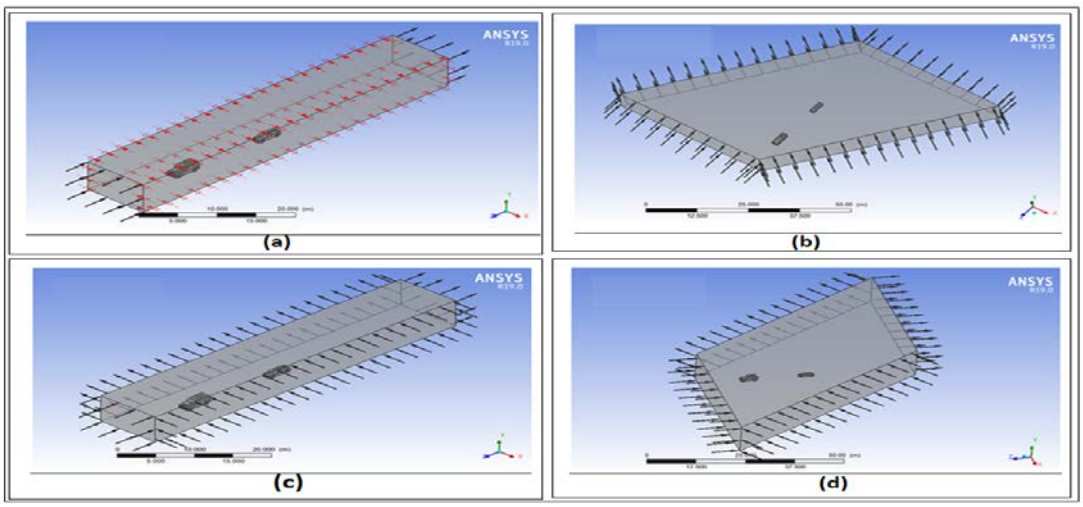


**Figure 4.** States inlet air with angles, (a) the influence of wind at State1; (b) the influence of wind at State 2; (c) the influence of wind at State3; (d) the influence of wind at State 4.

RESULTS AND DISCUSSION

Pressure distribution:

Figure5a. State 1 displays the pressure propagation effect on the vehicle's surface with a wind velocity of 80 km/h and a distance of 5 m between vehicles. In the front section, it has been found that there is a greater concentration of pressure on the vehicle. As it reaches the car's front section, the airflow will slow down and result in the air collecting in a narrower room. It can flow to lower pressure areas such as the head and windshield, sides, and bottom of the vehicle until the air stagnates in the frontal region of the vehicle. The friction reduces as the air flows over the head of the car. However, the pressure raises as it hits the windscreen—Figures5 b. State2 displays the pressure distribution effect on the vehicle's surface with a flow angle of 35o to two inlets for (front one and wall with a slip angle of 35o)and a wind velocity of 80 km/h. When the higher pressure air passes over the windshield in front of the windshield, it accelerates, allowing the pressure to decrease. lately, this lower pressure generates a lift force on the car roof as the air flows through it. Figures5c. State 3 two inlets demonstrated (front one and wall with a slip angle 90o) and wind speed is 80 km/h It has been demonstrated that there is a greater pressure concentration on the vehicle in the front portion and on the side mirrors of the car due to the intrusion of air into the front and wall with a 35-degree slip angle due to the entry of air into the front and wall. Figures5d depict State 4 displays the pressure transfer impact contour on the vehicle surface with a flow angle of 125-degree, two inlets here (front one and wall with slip angle125o). And the wind velocity is 80km/h, it has been seen that in the front portion there is a higher pressure concentration on the car and with the rising yaw angle the windward side was expanding. And the lateral force will rise. Figures 6 and 7 it has been shown that the pressure propagation effect on the surface of the vehicle with a wind velocity is 80 km/h with a distance of 10 m and 15 m between vehicles For the rear car ( front wheels and front of the bumper), the pressure at the stagnation point is lower compared to the front car and the reason for this can be found. Since the stream is separated from the surface during the passage from the front vehicle to the passage from the roof to the rear of the vehicle, and the separation is created on the rear windshield, which produces the low-pressure region on the rear glass and backside of the vehicle. As a consequence, a current of less pressure reaches the front side of the rear car than the inlet stream to the front car.

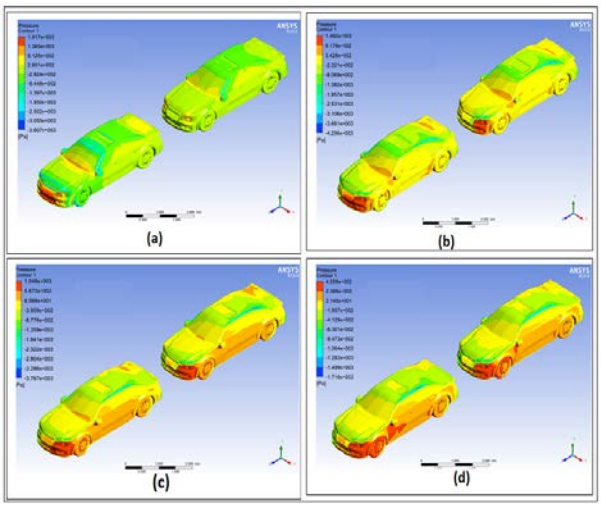


**Figure 5.** Pressure contour of two Chrysler cars with distance 5m, (a) the influence of wind at State1; (b) the influence of wind at State 2; (c) the influence of wind at State3; (d) the influence of wind at State 4.

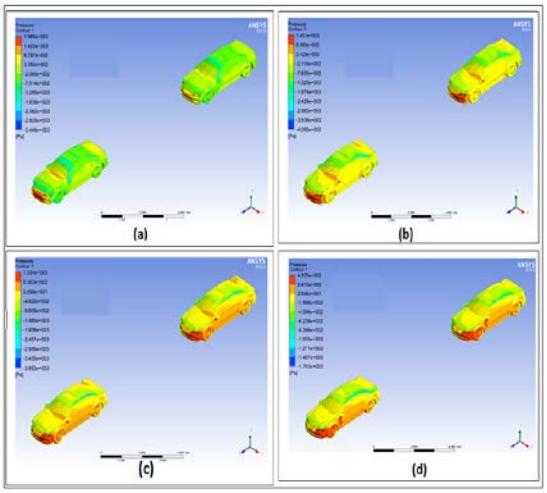


**Figure 6.** Pressure contour of two Chrysler cars with distance 10m, (a) the influence of wind at State1; (b) the influence of wind at State 2; (c) the influence of wind at State3; (d) the influence of wind at State 4.

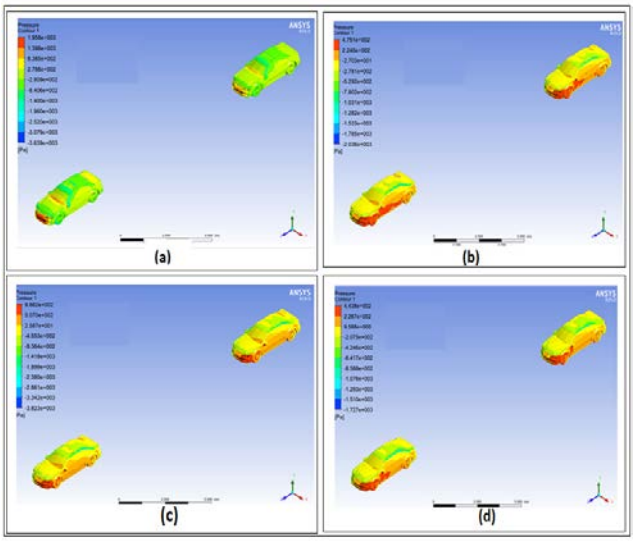


**Figure 7.** Pressure contour of two Chrysler cars with distance 15m, (a) the influence of wind at State1; (b) the influence of wind at State2; (c) the influence of wind at State3; (d) the influence of wind at State 4.

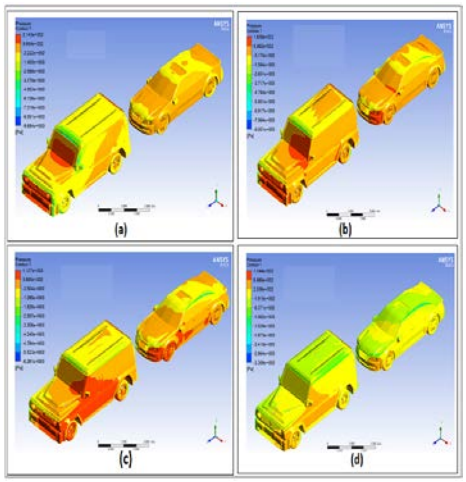


**Figure 8.** Pressure contour of Chrysler car tracked Mercedes G-class car with distance 5m, (a) the influence of wind at State1; (b) the influence of wind at State 2; (c) the influence of wind at State3; (d) the influence of wind at State 4.

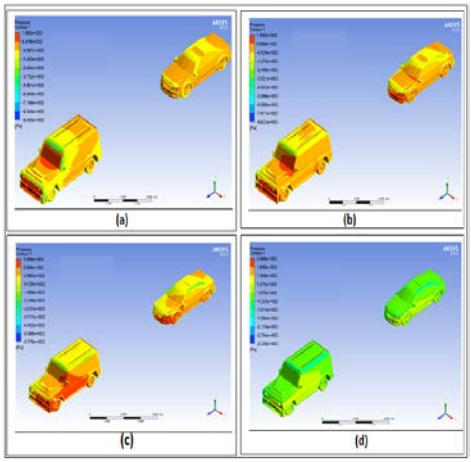


**Figure 9.** Pressure contour of Chrysler car tracked Mercedes G-class car with distance 10m, (a) the influence of wind at State1; (b) the influence of wind at State 2; (c) the influence of wind at State3; (d) the influence of wind at State 4.

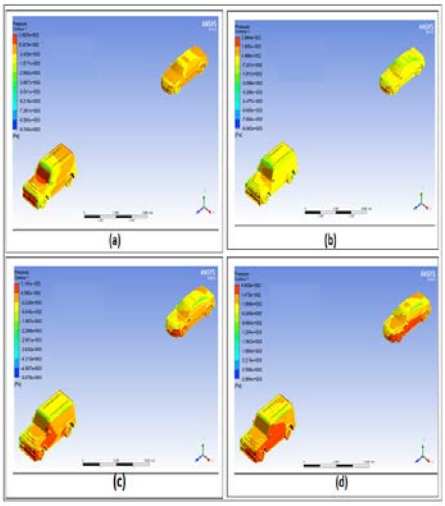


**Figure 10.** Pressure contour of Chrysler car tracked Mercedes G-class with distance 15m, (a) the influence of wind at State1; (b) the influence of wind at State 2; (c) the influence of wind at State3; (d) the influence of wind at State 4.

Figures 8,9, and 10. illustrates the pressure contours of Chrysler car tracked Mercedes G-class with distance (5m,10m, and 15m) between their centers with (0º,35º, 90º, and 125º). It is observed that the maximum pressure is 2844 Pascal when a distance of 15m at an angle of 125 degrees in front of the vehicle.

Velocity distribution

The velocity distribution in figures 11,12, and 13 represent the velocity contour of Chrysler cars with distance(5m,10m, and 15m) between their centers with angles with (0º,35º, 90º, and 125º), figures 14,15, and 16 represent the velocity contour of Chrysler car tracked Mercedes G-class car with distance (5m,10m, and 15m) between theme with angles with (0º,35º, 90º, and 125º), it can be observed that the magnitude velocity contours with the entire domain around the body of Chrysler. Maximum distribution of velocity at angle 0º and lowest distribution of velocity at angle 125º for all cases. The result shows the front portion of the vehicle and the rear of the car, the effect indicates the air velocity is decreasing. The air velocity rises from the front of the vehicle to the roof of the slide.

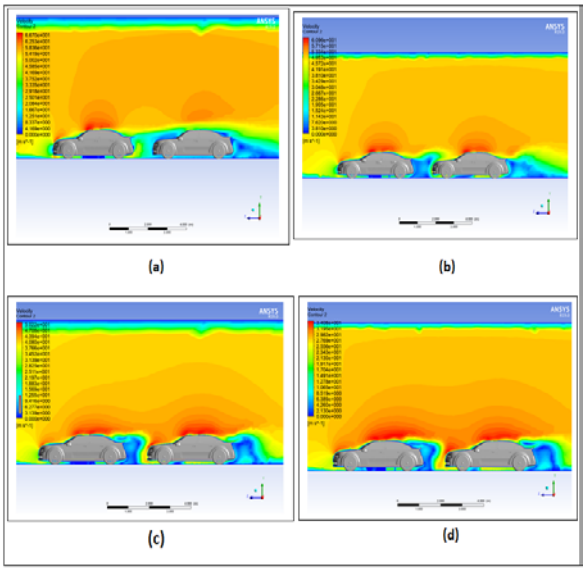


**Figure 11.**Velocity contour of two Chrysler cars with distance 5m, (a) the influence of wind at State1; (b) the influence of wind at State 2; (c) the influence of wind at State3; (d) the influence of wind at State 4.

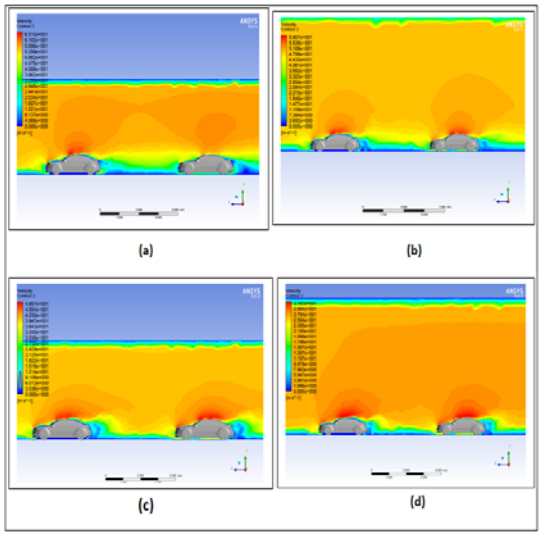


**Figure 12.** Velocity contour of two Chrysler car tracked another Chrysler car with a distance of 10m, (a) the influence of wind at State1; (b) the influence of wind at State 2; (c) the influence of wind at State3; (d) the influence of wind at State 4.

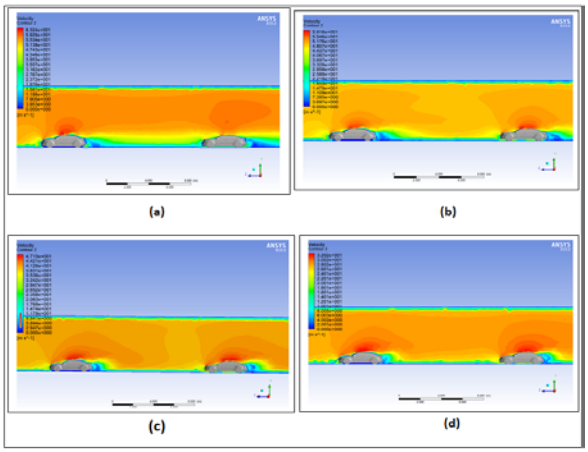


**Figure 13.** Velocity contour of two Chrysler cars with distance 15m, (a) the influence of wind at State1; (b) the influence of wind at State 2; (c) the influence of wind at State3; (d) the influence of wind at State 4.

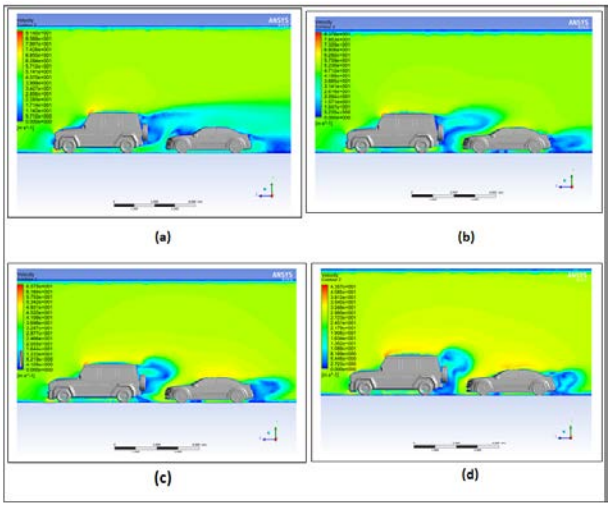


**Figure 14.** Velocity contour of Chrysler car tracked car Mercedes G-class car with distance 5m, (a) the influence of wind at State1; (b) the influence of wind at State 2; (c) the influence of wind at State3; (d) the influence of wind at State 4.

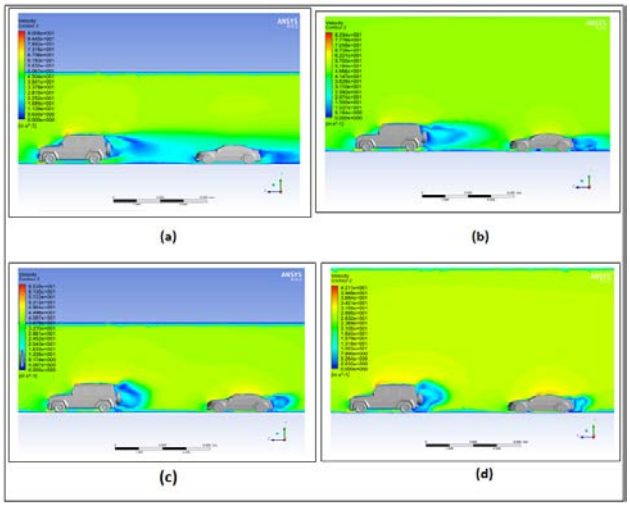


**Figure 15.** Velocity contour of Chrysler cars tracked car Mercedes G-class car with distance 10m, (a) the influence of wind at State1; (b) the influence of wind at State 2; ( c) the influence of wind at State3; (d) the influence of wind at State 4.

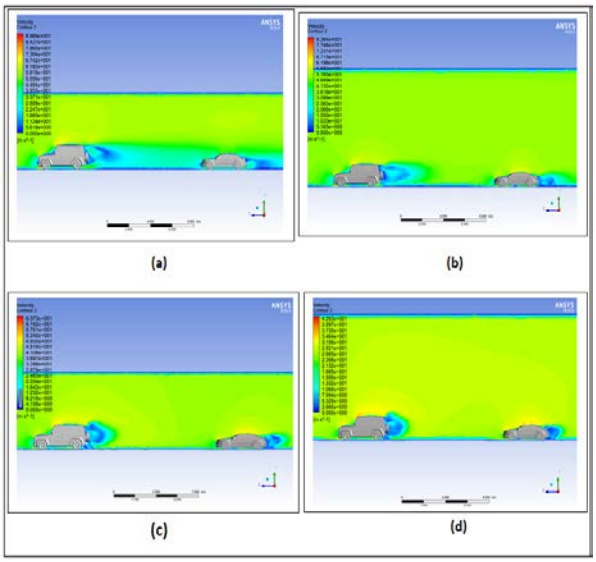


**Figure 16.** Velocity contour of Chrysler car tracked car Mercedes G-class car with distance 15m, (a) the influence of wind at State1; ( b) the influence of wind at State 2; (c) the influence of wind at State3; (d) the influence of wind at State 4.

Drag Force

The passenger car when tracked for an SUV with three distances of (5m,10m, and 15m) from their centres at one entry and one air raid on the cars, the drag force on the front car decreases when decrease distance between the two-car because the approaching back car helps in forming say a continuous body action. This action serves to keeping the streamlines attached, the aerodynamic conduct of the system is somewhat unstable at a distance of 5 meters from centres, since the short distance does not allow a continuous wake flow which generates high oscillation and turbulence, the front vehicles generates significant wake region including large eddies owing to the design of the G-class. When the back Chrysler car approaches to the G-class, it undergoes to these strong oscillations However, aerodynamics are decrease. As the waking flow behind the vehicles will follow a more constant and less noisy current, the aero dynamical behaviour at 10 meters is better than at 5 metres. At 15m, the lowering of the drag force still exists, but the lower gaps are not enough.

In this situation, the flow of air behind the trucks is stable and begins to fade away., as well as the drag force for the rear car decrease because of the challenge of air resistance on the first car. while when Chrysler car tracks another Chrysler car when neglected air velocity with velocity (70,100, and 130) km/h this state validity behaviour of the numerical data was confirmed with [3] It is noticeable that the value of drag force on the front car declines as soon as the rear car gets closer to the front car and, on the other hand, the value of drag force on the front car is much closer to the results of single-vehicle (S V), the reason it is on the fact that the creation on the front of the rear vehicle a high-pressure area, which produces a backside high-pressure area for the front car and reduces the pressure gap between the front side and the back of the front car. these analyses are shown in figure17, and the drag force on the rear car is less than the front car, because this may refer to that the design of Chrysler class does not generate significant wakes, moreover it provides less flow region. Hence the back approaching car exhibit less drag when it subjects to this low flow region, shown in figure18.

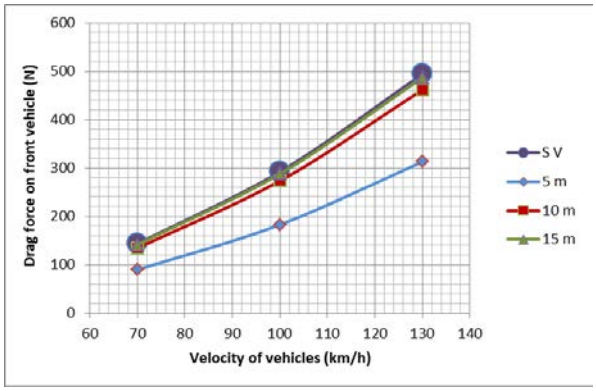


**Figure 17.** Drag force on front vehicle in different velocities and distances.

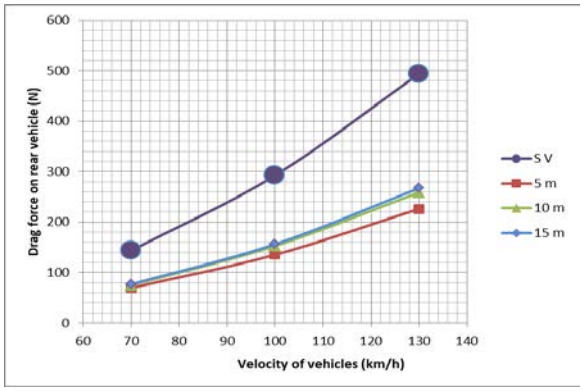


**Figure 18.** Drag force on rear vehicle in different velocities and distances.

Table1 shows the percentage decrease in the drag force of a Chrysler car when tracking another Chrysler car and when tracking a Mercedes G-Class with three distances (5m,10m, and 15m) between their centers with air intake angles (0º,35º, 90º, and 125º) when airspeed is 80 km/h and vehicles velocity is 120 km/h compared to single vehicle at the same angles. Show when the wind faces the two tandem cars at different angles, the drag force for the passenger car is reduced compared to a single-vehicle when the wind faces it at the same angles.

**Table 1.** The percentage decrease in the drag force of a Chrysler car when tracking another Chrysler car and when tracking a Mercedes G-Class with three distances (5m,10m, and 15m).

| Distance (m) | angle | Chrysler tracking another Chrysler | Chrysler tracking a Mercedes G- Class |
|---|---|---|---|
| | 0º | 28.7% | 51.8% |
| 5 | 35º | 21% | 33% |
| | 90º | 25% | 26% |
| | 125º | 57% | 44% |
| | 0º | 45.7% | 47% |
| 10 | 35º | 3.2% | 12% |
| | 90º | 2% | 15% |
| | 125º | 3.7% | 17.6% |
| | 0º | 26 | 45% |
| 15 | 35º | 5.6% | 15% |
| | 90º | 1% | 21% |
| | 125º | 6.5% | 28% |

Reactions force on tires:

Table 2 shows The forces acting on the front tires [the front right tire (Tire FR) and the front left tire (Tire FL)] of the Chrysler car in case of movement when tandem with another Chrysler car and when tandem with a Mercedes G-Class with three distances (5m,10m, and 15m) between their centers with air intake angles (0º,35º, 90º, and 125º) when air velocity is 80 km/h and vehicles velocity is 120 km/h, showed that the largest value of the reaction force of the front tires is on the front right tire (Tire FR) of the passenger vehicle at an angle of 35o and a distance of 15 meters between the two tandem cars.

**Table 2.** The forces that impact the vehicle's tires in the event of acceleration while the vehicle is driving. a Chrysler car when tracking another Chrysler car and when tracking a Mercedes G-Class with three distances (5m,10m, and 15m).

| Distance (m) | angle | Chrysler tracking another Chrysler | | Chrysler tracking a Mercedes G-Class | |
|---|---|---|---|---|---|
| | | Tire FL (N) | Tire FR (N) | Tire FL (N) | Tire FR (N) |
| 5 | 0º | 19.5629 | 19.6868 | -2.09612 | -1.46158 |
| | 35º | -19.1898 | 29.9898 | -23.8899 | 37.7009 |
| | 90º | -33.7841 | 46.6212 | -35.693 | 41.7177 |
| | 125º | -19.6132 | 20.9426 | -21.1216 | 15.9378 |
| 10 | 0º | 29.9924 | 28.6636 | 8.8916 | 14.1219 |
| | 35º | -29.2601 | 95.3639 | -21.6692 | 73.8335 |
| | 90º | -38.4044 | 77.3243 | -36.8886 | 71.1962 |
| | 125º | -19.3709 | 29.4182 | -26.4608 | 17.825 |
| 15 | 0º | 31.2027 | 28.9128 | 13.0773 | 14.059 |
| | 35º | -29.2494 | 107.542 | -33.4622 | 88.8012 |
| | 90º | -34.0653 | 69.6308 | -39.6821 | 79.0117 |
| | 125º | -17.4704 | 25.7809 | -25.0115 | 24.5762 |

## CONCLUSIONS

The disturbance of the wind at many angles on the vehicle and its effect when the passenger car tandem with the SUV vehicle and when it tandem with another particular distance Chrysler vehicle. In all States, the highest airflow rates occur as the wind faces vehicles with a 0-degree slip angle centered along the segment of the car. The highest pressure spread is registered when the wind faces the passenger vehicle when the SUV car is tandem with a distance of 15 m at a slip angle of 125 degrees centered around the section of the car. when a passenger car tandem another passenger car, and when it tandem with an SUV car the drag force on the front car decreases when decrease distance between the two-car and the drag force of the rear car less than on the front one. As well as when the wind faces the vehicles with different slip angles Chrysler's drag force is reduced compared to a single-vehicle.

## REFERENCES

[1] G.K. Rajamani, "CFD Analysis of Air Flow Interactions in Vehicle Platoons," Manuf. Eng., 2006.

[2] P. Ramya, A.H. Kumar, J. Moturi, and N. Ramanaiah, 2015, "Analysis of Flow over Passenger Cars using Computational Fluid Dynamics," Int. J. Eng. Trends Technol., Vol. 29, No. 4, Pp. 170–176, 2015. doi: 10.14445/22315381/ijett-v29p232.

[3] R.B. Kazerooni, M. Momenifar, K. Karimizad, and M. Afshar, "Investigation of Aerodynamic Forces on Two Tandem Cars," Pp. 10, 2015. doi: 10.1615/ichmt.2014.intsympconvheatmasstransf.300.

[4] J. Liu, C. Zhuang, S. Liu, and H.M. Zhou, "Numerical simulation of heavy truck's aerodynamic noise," IOP Conf. Ser. Mater. Sci. Eng., Vol. 657, No. 1, 2019. doi: 10.1088/1757-899X/657/1/012070.

[5] X. He, T. Li, C. Xi and H. Zhang, "Research on Underbody Flattening of a Passenger Vehicle towards Aerodynamics Optimization," IOP Conf. Ser. Mater. Sci. Eng., Vol. 517, No. 1, 2019. doi: 10.1088/1757-899X/517/1/012006.

[6] A. Hammad, T. Xing, A. Abdel-Rahim, V. Durgesh, and J.C. Crepeau, "Effect of Crosswinds on the Aerodynamics of Two Passenger Cars Crossing Each Other," Int. J. Automot. Technol., Vol. 20, No. 5, Pp. 997–1008, 2019. Oct., doi: 10.1007/s12239-019-0094-8.

[7] L. Prabhu, S. Krishnamoorthi, P. Gokul, N. Sushan, P.H. Hisham, and A. Jose, "Aerodynamics analysis of the car using Solidworks flow simulation with rear spoiler using CFD," IOP Conf. Ser. Mater. Sci. Eng., Vol. 993, Pp. 012002, 2020. doi: 10.1088/1757-899x/993/1/012002.

[8] A.A. Markina, A.D. Lukashuk, S.N. Chepkasov, and A.V. Starovoytenko, "Improving aerodynamic characteristics for drag reduction of heavy truck," IOP Conf. Ser. Mater. Sci. Eng., Vol. 862, No. 3, 2020. doi: 10.1088/1757-899X/862/3/032032.

[9] P. Kesuma, S. Darmawan, and A. Halim, "Aerodynamics Analysis of Mobil Irit Tarumanagara using CFD Method," IOP Conf. Ser. Mater. Sci. Eng., Vol. 1007, Pp. 012032, 2020. doi: 10.1088/1757-899x/1007/1/012032.

[10] A. Basit, R. Septian, and M. Royana, "Aerodynamic analysis and car body optimalization of saving energy 'wARAK' using software Ansys Fluent R15.0," IOP Conf. Ser. Mater. Sci. Eng., Vol. 788, No. 1, Pp. 0–10, 2020. doi: 10.1088/1757-899X/788/1/012073.

[11] O. Arteaga, "Aerodynamic optimization of the body of a bus," IOP Conf. Ser. Mater. Sci. Eng., Vol. 872, No. 1, 2020. doi: 10.1088/1757-899X/872/1/012002.

[12] H.J. Abid and A.A. Hussein, "Investigation on effecting parameters of the wind disturbance on stability of the steering system," Int. Rev. Mech. Eng., Vol. 14, No. 5, Pp. 331–338, 2020. doi: 10.15866/ireme.v14i5.18831.

[13] S. Aoki and R. Rajkumar, "A merging protocol for self-driving vehicles," Proc. - 2017 ACM/IEEE 8th Int. Conf. Cyber-Physical Syst. ICCPS (part CPS Week), pp. 219–228, 2017. doi: 10.1145/3055004.3055028.